Available online at www.sciencedirect.com
ScienceDirect
Wear 265 (2008) 477–489
WEAR
www.elsevier.com/locate/wear

Run-in behavior of nanocrystalline diamond coatings studied by *in situ* tribometry

Richard. R. Chromik [a,b,1], A. Leigh Winfrey [a], Jan Lüning [c], Robert J. Nemanich [a,d], Kathryn J. Wahl [b,*]

[a] *North Carolina State University, Department of Physics, Raleigh, NC 27695, USA*
[b] *U.S. Naval Research Laboratory, Code 6176, Tribology Section, Washington, DC 20375, USA*
[c] *Université Pierre et Marie Curie, 75005 Paris, France*
[d] *Arizona State University, Department of Physics, PO Box 871504, Tempe AZ 85287-1504, USA*

Received 3 October 2006; received in revised form 28 October 2007; accepted 30 November 2007
Available online 24 January 2008

Abstract

The friction performance of nanocrystalline diamond coatings was evaluated using *in situ* tribometry with sapphire counterfaces. Coatings were grown by microwave plasma assisted chemical vapor deposition in an Ar–H–CH_4 plasma, with H ranging from 0 to 36%. *In situ* examination of the sliding contact, combined with *ex situ* analysis of the sapphire counterface revealed that the velocity accommodation mode was interfacial sliding of a carbonaceous transfer film versus the coating wear track. For most tests, the contact diameter increased during the first 50 sliding cycles and then remained constant. The *in situ* measure of the contact diameter was found to correlate confidently to *ex situ* measurements of counterface wear. The performance of the diamond coatings, characterized by quick run-in to low friction was best when a small but detectable graphite peak was present in the X-ray diffraction (XRD) profile. The relative intensity of the XRD graphite peak was also found to directly correlate with the peak position of the C1s $\rightarrow \pi^*$ transition as measured by near-edge X-ray absorption fine structure (NEXAFS) spectroscopy. Increasing the relative amount of graphite-bonded sp^2 carbon in the NCD films decreased run-in cycles to low friction.

Keywords: Diamond; Friction; Nanocrystalline diamond; *In situ* tribometry; Wear; NEXAFS

1. Introduction

With significant evidence for robust mechanical properties [1–5] and good tribological performance [6–10], nanocrystalline diamond (NCD) has become a coating with applications from machine tools to micro-electro-mechanical systems (MEMS) [1,6–8,10,11]. The challenge of reducing the surface roughness of traditional CVD-grown microcrystalline diamond coatings (MCD) has been practically eliminated with the development of new growth processes. Pre-nucleation techniques and various gas mixtures including H, Ar and methane have been shown to result in diamond grain sizes in the range of 2–10 nm and RMS surface roughness below 50 nm [1,12–18]. Despite this advance, recent tribological studies on NCD coatings showed a period of initially high friction ("run-in") before low friction coefficients were achieved [6,10]. For NCD to be used as a MEMS material, low friction with minimal run-in is desired. These conditions would address design concerns and allow for on-chip actuators that are smaller and consume less power.

Run-in behavior is often correlated to the initial interactions between the asperities of two surfaces. This process results in locally high contact stresses that lead to plastic deformation, wear and the creation of third-bodies [19,20]. For a solid lubricant coating, the reduction in friction following this stage is typically associated with the formation of a stable transfer film [20,21]. Diamond also follows this trend of high friction run-in with wear followed by low friction. It has been speculated that the low friction mechanism for diamond is the formation of a thin, less-dense carbon transfer layer, possibly graphitic in nature [22–24].

Many tribological studies on MCD coatings have recognized that surface roughness plays a critical role for run-in and

* Corresponding author. Tel.: +1 202 767 5419; fax: +1 202 767 3321.
E-mail address: kathryn.wahl@nrl.navy.mil (K.J. Wahl).
[1] Present address: McGill University, Department of Mining and Materials Engineering, 3610 University Street, Montreal, QC, Canada H3A 2B2.

0043-1648/$ – see front matter © 2007 Elsevier B.V. All rights reserved.
doi:10.1016/j.wear.2007.11.023

the eventual steady-state friction [22,25–29]. For diamond on diamond sliding, low friction and short run-in has only been achieved on highly polished diamond coatings. Other counterface materials can result in departures from this behavior. For example, Hayward's studies [26] of sapphire versus diamond sliding under environmental conditions similar to this study demonstrated that the roughness of the diamond coating affected the wear of the sapphire counterface as well as the friction properties. Low friction was eventually observed, but at the expense of extensive counterface wear. Bull et al. [28] conducted a similar study of sapphire sliding versus MCD coatings and found a regime of continuous high friction ($\mu \sim 0.65$) that was independent of coating roughness. The difference between these two studies may be a reflection on the quality of the various diamond coatings, possibly with respect to their ability to form a transfer film and act as a solid lubricant coating [21].

In this study, we examine the tribology of nanocrystalline diamond coatings grown in Ar–H–CH_4 plasmas with H content ranging from 0 to 36%. An *in situ* tribometer with a sapphire counterface was used, allowing for examination of the sliding contact and identification of velocity accommodation modes (VAM) [20,21]. Performance of the NCD coatings was characterized by both the extent of high friction run-in and measurements of the *in situ* contact diameter, a quantity tied to counterface wear. Coating performance was also linked to coating roughness, chemistry, microstructure, and the formation of transfer films on the sapphire counterfaces.

2. Experiment

Nanocrystalline diamond coatings were prepared using a microwave plasma enhanced chemical vapor deposition system (1.5 kW ASTeX 2.45 GHz). The gases used for deposition were Ar, H_2, and CH_4. Coatings were deposited on single side polished silicon (1 0 0) wafers after a seeding process. Samples were grown at 900 °C and with a microwave power of 900 W in a chamber at 65 Torr. The total gas flow was 70 sccm with CH_4 flow set to 7 sccm for all coatings. Flow rates of argon and hydrogen were varied from sample to sample, with the hydrogen ranging from 0 to 36% of the total gas flow. The coatings discussed in this study are denoted to by the percent of hydrogen in their growth plasma:

$$H^{\#} = \frac{[H_2]}{([H_2] + [Ar] + [CH_4])}. \quad (1)$$

The $H^{\#}$ refers to the percent of hydrogen gas in the total flow of gasses during coating growth. Bracketed quantities are the flow rates of the feed gasses during the growth process. The hydrogen flow rates were: 0, 6, 7, 10, and 25 sccm, and the argon flow rates were 63, 57, 56, 53, and 38 sccm, where each of the quantities represent the flow rates of the specific gases. Based on these flow rates and Eq. (1), five different coatings were prepared: H0, H8.5, H10, H14 and H36.

X-ray diffraction was conducted on the coatings using a standard $\theta - 2\theta$ geometry with 3 degree offset of the goniometer axes to minimize the intensity of the Si substrate peak. The X-ray radiation was Cu, filtered with a Ni foil such that the wavelength, λ, was 0.15418 nm. Samples were examined over the range of $2\theta = 20$–100 degrees. Diffraction peaks were fit to a Lorentzian function using standard peak-fitting software. From these measurements, the average lattice spacing and two estimates of the grain size were calculated. First, the method of integral breadths [30], also called the Williamson–Hall plot method [31], was applied using the relation:

$$\beta_{1/2} \cot \theta = \frac{0.9\lambda}{D \sin \theta} + 4\varepsilon \quad (2)$$

where $\beta_{1/2}$ is the full-width half-maximum (FWHM) of the peak and θ is the half the detector angle for the peak position. Estimates of the grain size and the lattice strain, ε were found from a linear fit to a plot of $\beta_{1/2} \cot \theta$ versus $1/\sin \theta$. Additionally, the Scherrer formula was used to calculate a grain size, D, from the (1 1 1) diamond peak:

$$D = \frac{0.9\lambda}{\beta_{1/2} \cos \theta}. \quad (3)$$

The Scherrer formula may be derived from Eq. (2) with an assumption of zero lattice strain. Other researchers that have studied CVD diamond coatings have found that the stress state of their coatings is complex [32–35], possibly due to twinning [34,35]. This leads to additional broadening of the X-ray lines that makes Eq. (2) difficult to apply. For this reason, we report the results of both methods.

Near edge X-ray absorption fine structure (NEXAFS) spectroscopy was used for quantitative determination of the elemental and chemical bonding environment yielding, in particular, the sp^2 to sp^3 carbon ratio. NEXAFS spectra were recorded at the wiggler beam line 10–1 of the Stanford Synchrotron Radiation Laboratory (SSRL) over the photon energy range of 270–470 eV by monitoring the sample's total electron yield (TEY) signal. The number of incoming photons was monitored by the TEY signal of an 80% transmissive Au net. Both drain currents were recorded with a Keithley 427 Current Amplifier. The ratio of sample signal and incoming photon flux is the TEY spectrum, which is a good approximation proportional to the sample's absorption coefficient [36,37]. As discussed in the literature [36], experimental spectra were normalized to a common edge jump. The absolute energy scale was established by referencing the first transmission dip due to carbon contamination of the beam line optics to 284.7 eV.

The morphology of as-prepared coatings and wear tracks were examined in a LEO Supra50 scanning electron microscope. The accelerating voltage was either 5 or 10 keV. Qualitative chemical identification was carried out with an Oxford Instruments energy dispersive spectrometer (EDS). Additional examination of the sample morphology was carried out with a Veeco Nanoman Dimension series atomic force microscope (AFM). The instrument has closed loop scanning capabilities for quantitative analysis of surface topography and roughness characterization. Scans were conduced at varying sizes ranging from 1 to 40 μm. The roughness values reported here were calculated from the 10 μm scan size images acquired

using nominally 20 nm radius tips in intermittent contact mode.

Reciprocating sliding tests were conducted using a custom-built *in situ* tribometer [21,38] designed to operate underneath an optical microscope. Direct observation of the contact region was conducted for all tests by using a transparent sapphire counterface. A 6.35 mm diameter sapphire hemisphere was loaded against a nanocrystalline diamond coating via a fixed load on a lever arm. The normal load on the coating was 6.4 N and resulted in an initial average Hertzian contact stress of 0.7 GPa. Friction tests were performed at room temperature in humid air (35–45% RH) up to 1500 cycles. All tests were run at a sliding speed of 1 mm/s over an initial track length of 6 mm. As the test progressed, the track length was shortened to 4 mm at cycle 100.

The friction force was measured from a calibrated piezoelectric force sensor housed in the sample stage. Data acquisition was conducted such that spatially resolved friction was measured across the track at 20 μm intervals. Average friction coefficients for a given cycle were determined from the central 10 to 90% of the track length from the average friction force divided by the normal load. Steady-state friction values are calculated by averaging the last 200 data points of a test. Average steady-state values for a given coating are reported from the average among 3 tests conducted on that coating. A period of high friction (run-in) occurred at the start of each test. When the friction reached a low value, typically $\mu < 0.1$, the friction was constant or only gradually changing. Thus, the number of cycles for run-in was determined by taking a derivative of the friction trace. The cycle number when the derivative became zero was taken as the point when run-in was complete.

Optical images of the sliding contact were captured through the sapphire counterface with a Nikon 20x ultra-long working distance (ULWD) objective. Video of the test was recorded to both S-VHS video tape and to the hard drive of a DVD recordable unit. Image captures taken directly from the digital recording were used to make measurements of the mean contact diameter. Standard photo editing software was used, with the length scale calibrated using a 0.01 mm scale bar for optical microscopy.

Raman spectroscopy was performed on coatings and counterfaces using a Renishaw System 1000 Raman Microprobe. Two lasers were used. Visible Raman was conducted with an Ar+ ion laser (514 nm) focused to a spot of less than 2 μm. Near infrared was also conducted using a diode laser (785 nm) in line focus mode (~20 μm × 2 μm).

Ex situ measurements of coating wear tracks and counterface wear flats were conducted with stylus profilometry and non-contact profilometry. Wear track depths were measured with a Tencor P-10 stylus profiler with a 2 μm radius tip. Cross sectional wear areas were calculated by integrating the height profiles. Sapphire hemispheres were examined with a white light interferometric profiler (Zygo Newview 5000) with a 50× Mirau objective. A 3D height image of the wear scar was examined for all tests. Wear scar diameters were used to calculate a wear volume for the removal of a spherical cap from the sapphire counterface [39].

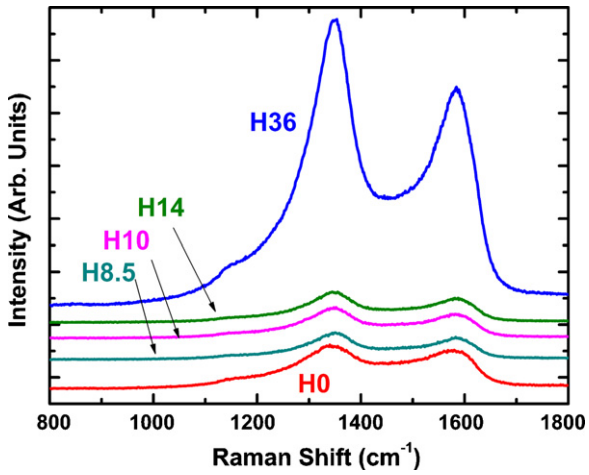

Fig. 1. Raman spectra for the NCD coatings taken with a 514 nm laser.

3. Results

3.1. Coating characterization

Typical Raman spectra for the NCD coatings are shown in Fig. 1. All spectra exhibited features associated with nanocrystalline diamond [16,40–44]. The spectral features are broad bands at 1350 and 1520–1580 cm^{-1} with shoulders at 1100–1150 cm^{-1} and 1430–1470 cm^{-1}. The large features around 1350 and 1580 cm^{-1} are the D and G modes characteristic of amorphous or diamond-like carbon. The 1150 cm^{-1} shoulder has been related to the presence of nanocrystalline diamond [41], as has the 1470 cm^{-1} shoulder [44].

X-ray diffraction scans for NCD coatings H0, H8.5 and H36 are shown in Fig. 2. All coatings studied exhibited the (1 1 1), (2 2 0) and (3 1 1) peaks for diamond with different intensity ratios. Thus, crystallographic orientation varied among the coatings studied. Using a qualitative analysis for diamond orientation [12], coatings H0, H10, H8.5 and H14 were all found to have a

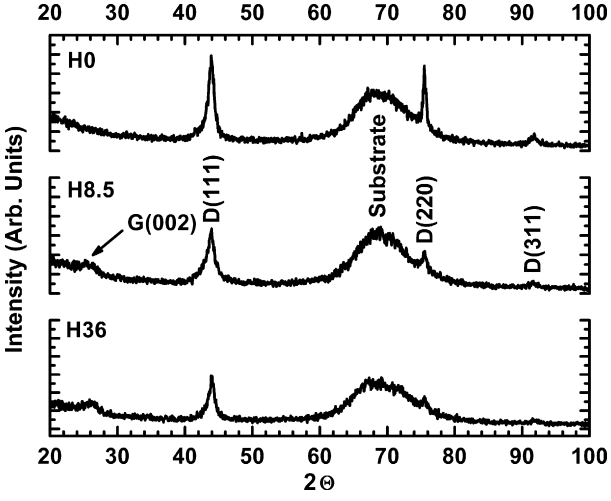

Fig. 2. X-ray diffraction results for H0, H8.5 and H36.

weak (1 1 0) texture. Coating H36 was found to be weakly (1 1 1) textured (see Table 1).

In Fig. 2, the scans for H8.5 and H36 also exhibited a broad, low intensity peak at roughly 26°, consistent with the (0 0 2) reflection for graphite. The peak appeared for all coatings except H0. The presence of this peak indicated a trace amount of nanocrystalline graphite in these NCD coatings. Using the Scherrer formula (Eq. (3)), the grain size was estimated as between 3 and 5 nm. The intensity of the graphite peak varied from sample to sample and is given in Table 1 normalized to the sum of diamond (2 2 0) and (1 1 1) peak intensities.

Further results from the X-ray diffraction studies revealed a number of key features regarding the NCD coatings. Grain size estimates, average lattice constant and estimated lattice strain are all listed in Table 1. For all samples, the lattice constant was found to be slightly less than the value of bulk diamond ($a = 0.35668$ nm), indicating that the stress state of the coatings was compressive. The method of integral breadths [30,31] was used to estimate the lattice strain. All samples exhibited negative (compressive) strain, consistent with the lattice constant results.

Grain size estimates from either the Scherrer or the Williamson–Hall method are generally considered to be a lower limit, especially when examining CVD diamond coatings. Both Silva et al. [35] and Fayette et al. [34] showed that the stress state of diamond coatings is complex and typically results in a non-linear trend on a Williamson–Hall plot. One reason for the complex stress in these coatings was determined to be twinning. This microstructural feature was shown to result in additional satellite peaks about the (1 1 1) X-ray reflection and additional broadening of the (1 1 1) line itself. Williamson–Hall plots for our specimens using the (1 1 1), (2 2 0) and (3 1 1) reflections resulted in confident fits except for coatings H0 and H14. Bachmann et al. [32] recognized the difficulty with the Williamson–Hall analysis and suggested that the Scherrer grain size is a better estimate. Based on our results in Table 1 and regardless of the analysis technique used, the estimated diamond grain size for the NCD coatings lies between 5 and 11 nm. XRD results are consistent with measurements from transmission electron microscopy (TEM) conducted on similar coatings [45].

NEXAFS spectra for the NCD coatings are shown in Fig. 3 along with the reference spectrum of HOPG. The peak around 285 eV corresponds to the excitation of C 1s electrons to the unoccupied π* states of sp^2 (C=C) hybridized carbon atoms present in particular in phenyl ring-like structures [36]. With changing deposition conditions (increasing H content in the source gas), the energy of the 1s to π* transition increased from 285.0 to 285.5 eV (values determined by peak fitting are reported in Table 1). Such a shift has been observed previously and attributed to transformation of the carbon sp^2 bonding environment from a disordered to graphitic-like structure in the coating [46,47]. These values are reported in Table 1. Transitions to σ* orbitals are located in the spectral region above 288 eV, which originate from C 1s transitions at C–C, C=C, and C≡C bonded sites to their respective, unoccupied σ* states [48]. The disordered nature of the coatings tends to spread the features of the σ* resonances from 289 to 310 eV, but the characteristic diamond

Table 1
Characteristics of the nanocrystalline diamond coatings determined from X-ray diffraction, NEXAFS and atomic force microscopy

Sample	AFM	NEXAFS	XRD (diamond peaks)					XRD (graphite peak)	
	RMS roughness (nm)	sp^2 content (%)/C1s → π* peak position (eV)	Grain size (nm) Scherrer	Grain size (nm) Williamson–Hall	D(1 1 1)/D(2 2 0)	Lattice strain ($\times 10^{-3}$)	Lattice constant (Å) (±0.005)	G(0 0 2)/D[(2 2 0) + (1 1 1)]	Grain size (nm) Scherrer
H0	28	11/284.97	10.5	8.1	1.4	−2.5	3.560	0	–
H8.5	30	20/285.29	7.2	4.8	2.7	−6	3.560	0.15	3.6
H10	26	16/285.20	8.4	5.7	2.1	−5	3.560	0.06	4.8
H14	40	14/285.30	8.2	7.2	2.6	−3	3.559	0.09	3.3
H36	78	15/285.48	8.2	9.6	3.9	−0.4	3.557	0.20	3.4

The peak ratio of D(1 1 1) to D(2 2 0) indicates preferred crystalline orientation, where a value of 3.4 indicates random texture.

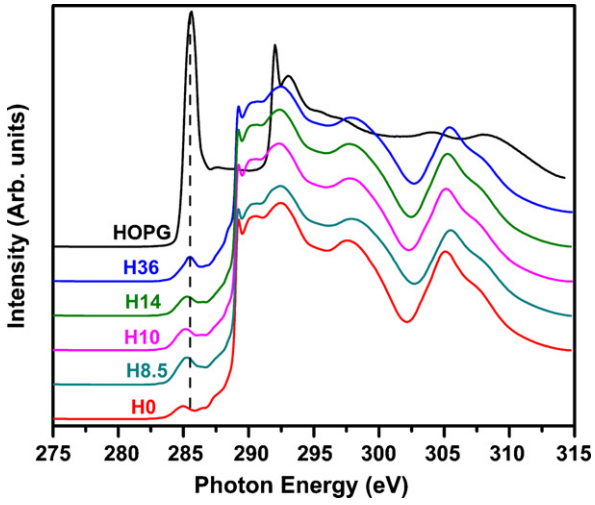

Fig. 3. NEXAFS spectra for the NCD coatings and a HOPG reference sample. The dashed vertical line marks a photon energy of 285.5 eV.

second band gap is clearly visible around 302 eV, maintaining the same overall shape for all samples.

Chemical bonding composition analysis to determine the fraction of sp^2 bonded carbon in the sample was carried out by a method described by Lenardi et al. [49]. For this the ratio of the peak areas of the 1s to π* resonance and a large part of the 1s to σ* portion of the spectra is compared to the same ratio in the pure graphite sample. For the π* peak we used the area from 282 to 288 eV and the area from 288 to 310 eV for the σ* portion of the spectrum. The sp^2 fraction is then determined using:

$$f_{sp^2} = \frac{I^{\pi^*}_{\text{sample}}}{I^{\pi^*}_{\text{HOPG}}} \frac{I_{\text{HOPG}}(\Delta E)}{I_{\text{sample}}(\Delta E)} \quad (4)$$

where $I^{\pi^*}_{\text{sample}}$ and $I^{\pi^*}_{\text{HOPG}}$ are the areas of the π* peak, evaluated from 282 to 288 eV, of the NCD sample and the HOPG reference, respectively. $I_{\text{sample}}(\Delta E)$ and $I_{\text{HOPG}}(\Delta E)$ terms are the σ* areas taken from 288 to 310 eV[48]. The calculated sp^2 percentages for the coatings studied are listed in Table 1.

Surface morphology of the coatings was fairly similar between coatings. Fig. 4 is an AFM image of H36. All samples exhibited clustered growth domains, often referred to as a "cauliflower-like" structure. Within the growth domains, a finer structure was noted that resembled a more needle-like morphology. These morphologies were observed both in AFM (Fig. 4(a) and SEM (Fig. 4(b)) imaging. Roughness measured by AFM is presented in Table 1; roughness increased with hydrogen content of the growth plasma. It was expected that the roughness of the coating would correlate with growth domain size rather than nanocrystalline grain size [50]. This study did not examine how these trends correlated with deposition conditions.

In summary, as the hydrogen content in the growth plasma was increased: (1) coating RMS roughness increased; (2) diamond grain size estimated from X-ray diffraction remained the same; (3) the intensity of the (0 0 2) graphite peak in XRD increased; (4) the C 1s → π* peak position shifted from 285.0 to 285.5 eV; and (5) the preferred crystalline orientation of the coatings changed from diamond (1 1 0) to diamond (1 1 1).

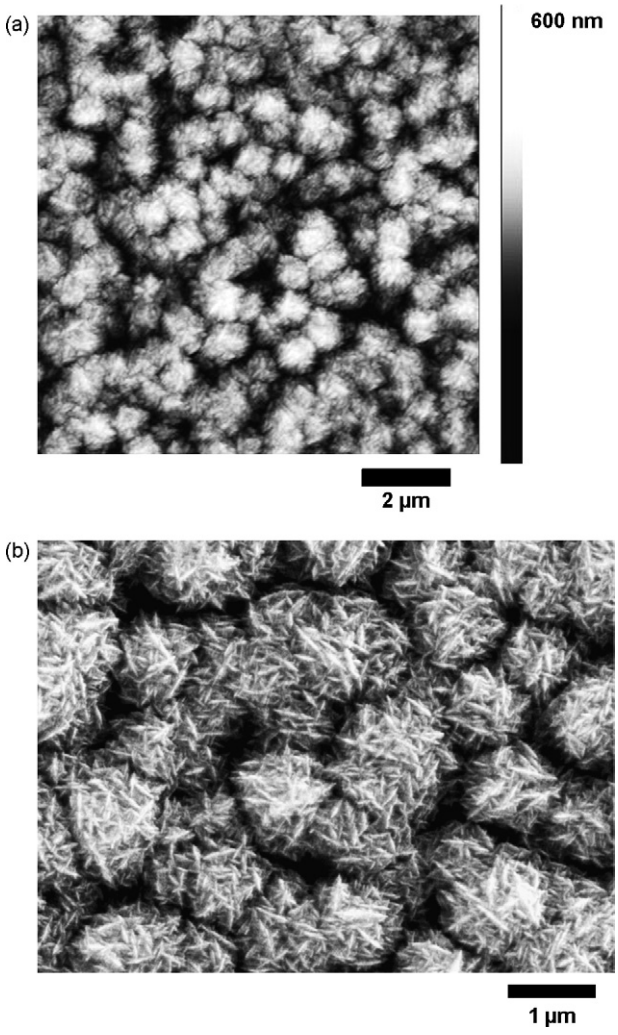

Fig. 4. Images of NCD coating H36 by (a) AFM and (b) SEM.

3.2. Tribology of NCD coatings

Average friction versus cycle number is plotted in Fig. 5 for individual tests on the nanocrystalline diamond coatings. The

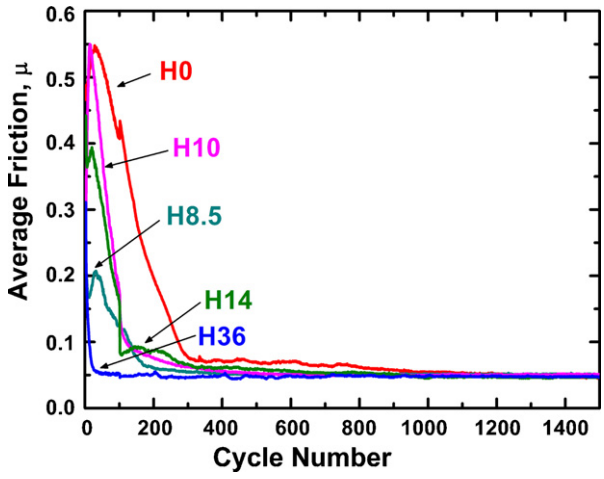

Fig. 5. Friction vs. cycles for reciprocating sliding tests on the NCD coatings.

Table 2
Results for tribological performance of the nanocrystalline diamond coatings

Sample	Cycles to run-in	Steady-state friction	Coating wear area (μm^2)	Counterface wear volume ($\times 10^3$ μm^3)	Cycles to steady-state contact diameter
H0 (LW15)	440 ± 100	0.05, 0.08, 0.1	3	27, 65, 71	50, –, –
H8.5 (LW16)	170 ± 30	0.049 ± 0.003	9	9 ± 5	50, 20, 50
H10 (LW17)	250 ± 30	0.046 ± 0.005	6	15 ± 2	30, 20, 50
H14 (LW18)	210 ± 50	0.055 ± 0.008	8	19 ± 2	20, 50, 50
H36 (LW22)	100 ± 50	0.048 ± 0.001	9	12 ± 5	20, 20, 20

run-in behavior was different for each coating, but in all cases a low steady-state friction of $\mu \sim 0.05$ was eventually reached. Table 2 lists the average cycles of run-in calculated from three tests on each coating. Sample H36 reached low friction most quickly, while sample H0 took the longest. Also, H0 did not always reach $\mu = 0.05$ in steady state. The steady-state friction for the two other tests run on H0 reached 0.08 and 0.1 for the final steady-state friction coefficients.

3.3. Ex situ analysis—wear tracks and transfer films

Wear tracks were examined by AFM, with selected tests also examined with contact profilometry. In general, wear tracks had a polished appearance (see Fig. 6 (b–d)). The reciprocating sliding process wore away much of the needle-like and cauliflower-like morphology that was apparent in as-prepared coatings (Fig. 6(a)). Coating H8.5 had an as prepared RMS roughness of 30 nm. Fig. 6 shows the wear tracks on this coating after 1, 100 and 1500 cycles. Even a single-pass track (see Fig. 6(b)) exhibited smoothing of the coating and a slightly reduced RMS roughness of 26 nm. Continued sliding resulted in lower RMS roughness values of 7.2 nm at 100 cycles and 6 nm at 1500 cycles. It is apparent that most of the smoothing took place in the first 100 cycles. Worn track regions for all coatings after 100 cycles exhibited roughness on the order of 5–10 nm. Profilometry measurements of the wear tracks run for 1500 cycles revealed cross-sectional wear rates on the order of 10^{-6} $mm^3/(N\,m)$ or less. Raw profilometry data indicated average wear track depths of no more than 50 nm for the coatings studied.

Chemical analysis of the wear tracks with EDS revealed a signal for Al both in the track and at the turn around points. Fig. 7(a) and (b) show the EDS data collected from two regions of a wear track on samples H0 and H36. Some evidence of Al is found in the track, but the majority of worn sapphire from the counterface was found as debris at the turn-around points. Thus, the smoothening of the coating observed in Fig. 6 was due mostly to diamond polishing but also from some sapphire left in the wear track. Fig. 7(c) shows the typical debris collected at the end of a wear track on coating H0.

Non-contact profilometry carried out on the sapphire counterfaces showed that a wear flat was generated by sliding against the diamond coatings. Fig. 8 is a profilometry scan on a counterface run against coating H36. A spherical cap of material was removed, whose volume was calculated from the diameter of this wear scar [39]. Table 2 lists average counterface wear volumes for testing against each NCD coating. Except for coating H0, the wear volume was similar for each of the three tests and an average is reported. For coating H0, the wear volumes differed significantly among the three tests, and were always higher than any individual measurement for the other coatings.

Ex situ Raman spectroscopy revealed evidence of a carbonaceous transfer layer on the sapphire counterfaces. Fig. 9 shows Raman spectrum (785 nm excitation) collected from the center of a wear scar for a test conducted on coating H36 and the spectrum from the as-prepared coating. The nature of the transfer film spectrum is qualitatively similar to the spectrum from the as-prepared coating. Similar spectra were obtained from the counterfaces used on other coatings. No evidence for an enhanced graphitic nature of the transfer film was found. In a study by Scharf et al. [38] on diamond-like carbon coatings, a secondary G band at higher wavenumber was found and interpreted as evidence of graphitic transfer film formation. For this study, a change in excitation wavelength from 514 to 785 nm was necessary to reduce a strong fluorescent background signal. The wavelength shift also reduced the sensitivity to the G band of carbon, possibly masking detection of a transformation to graphitic carbon [22–24]. From this Raman study of the sapphire counterfaces, we find that a carbonaceous transfer film forms that is similar to the parent NCD coating.

3.4. In situ observations

Examination of the sliding contact revealed that the contact diameter increased as the test progressed. Measurements of the contact diameter from an *in situ* image during the final sliding cycle correlated well with *ex situ* measurements by non-contact profilometry. Thus, the increase in the observed contact diameter was found to correspond directly to the wear of the sapphire counterface. Fig. 10 contains plots of contact diameter, as well as friction coefficient, versus sliding cycle for coatings H0, H8.5 and H36. For coating H0 (Fig. 10(a)), the contact diameter steadily increased throughout the test. Based on these measurements, the average contact stress fell to roughly 0.2 GPa at cycle 1500. During this test, a friction coefficient of 0.05 was never attained, and the steady-state friction was 0.08. While the friction was high, the sapphire counterface was continually wearing, apparent from the steadily increasing contact diameter.

The other NCD coatings typically reached a low friction in fewer sliding cycles than the test in Fig. 10(a) and correspondingly reached a steady-state contact diameter more quickly. This is depicted in Fig. 10(b) and (c) for coating H8.5 and H36,

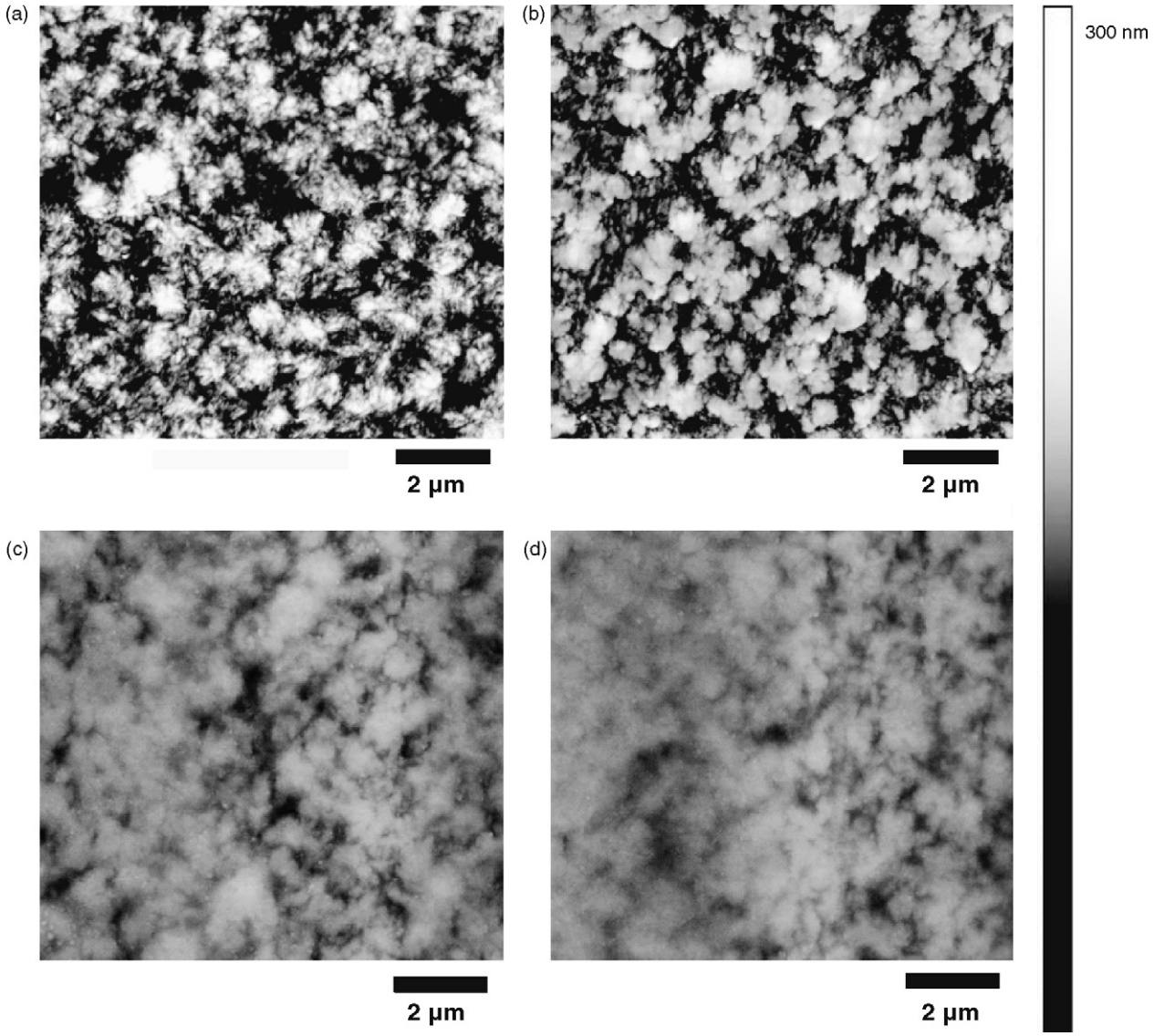

Fig. 6. AFM images of coating H8.5: (a) as prepared coating and wear tracks at (b) 1 cycle; (c) 100 cycles; and (d) 1500 cycles.

respectively. For coating H8.5, the contact diameter increased to 140 μm by cycle 50 and remained this size for the remainder of the test. This increase in contact diameter corresponded to a reduction in the average contact stress to roughly 0.4 GPa. A wear volume calculated from this *in situ* measurement, 6.6×10^3 μm^3, corresponded well with what was measured *ex situ* (see Table 2). Similarly, for the test on coating H36, the contact diameter increased to 145 μm by cycle 20 and was constant in size for the remainder of the test. The wear volume from this measurement is 8×10^3 μm^3, again in agreement with the *ex situ* results (Table 2).

Similar to the results presented in Fig. 10(b) and (c), most tests resulted in a rapid abrasion of the sapphire counterface (observed by an increase in contact diameter) followed by steady-state sliding of a wear flat versus the NCD coating. This wear behavior was observed for all coatings and did not depend on the magnitude of the friction during run-in or how long run-in lasted (e.g. the run-in for H36 was minimal but the sapphire still wore). An exception was coating H0, where, for two tests, a low steady-state friction of $\mu \sim 0.05$ was never reached. In these cases, as displayed in Fig. 10(a), the sapphire counterface wore throughout the test.

Observation of the sliding contact also allowed for determination of the velocity accommodation mode (VAM) [19–21]. Based on video imaging, wear debris was not observed to move within the contact region. However, *ex situ* Raman analysis identified that a carbonaceous transfer film does form. Based on these observations the VAM was found to be interfacial sliding of a thin transfer film versus the NCD coating. Interfacial sliding is a low energy VAM that typically results in low friction, especially for solid lubricant materials such as DLC or MoS_2 [21,38,51,52].

4. Discussion

For sapphire counterfaces sliding against nanocrystalline diamond coatings, low friction coefficients ($\mu \sim 0.05$) were typ-

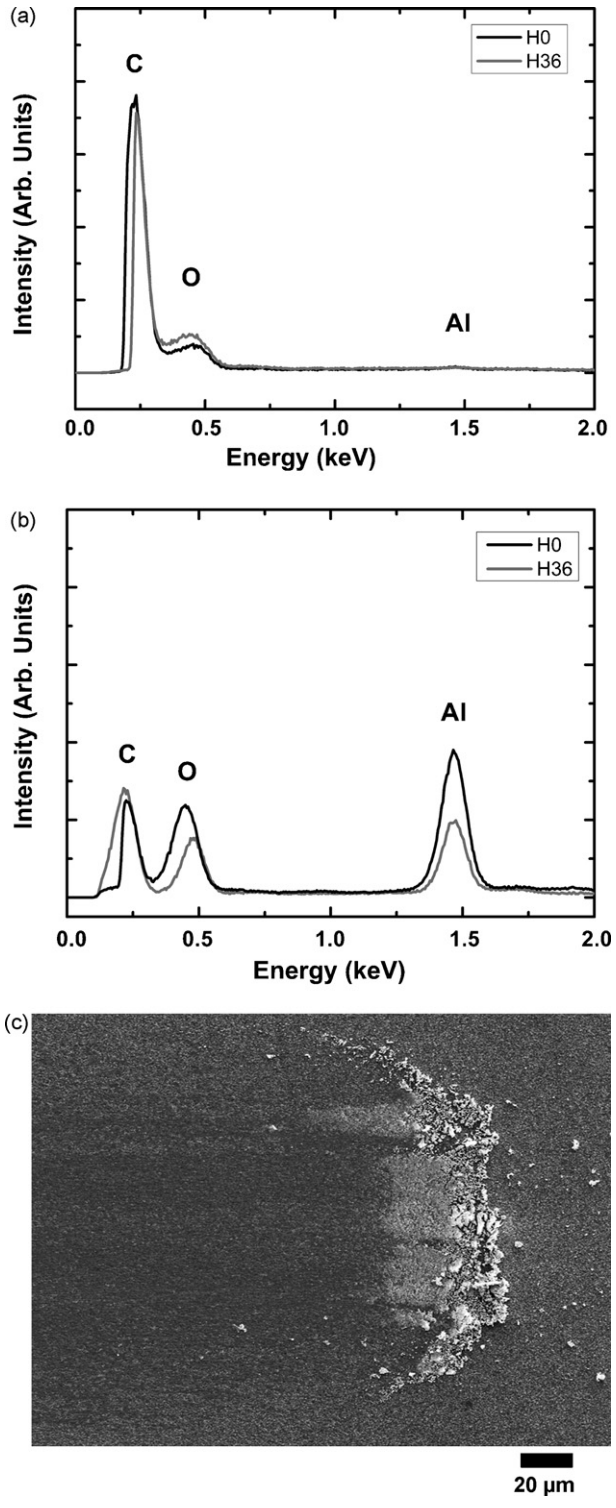

Fig. 7. EDS data for (a) wear tracks on coating H0 and H36, and for (b) endpatches on coating H0 and H36. Also, (c) an SEM image of an endpatch on coating H0.

ically observed after a run-in period of high friction. This result is different from previous studies of sapphire sliding against microcrystalline diamond (MCD) coatings. Bull et al. [28] found that sapphire sliding versus MCD coatings (40 nm < Ra < 80 nm) always had high friction. Similarly, Hayward et al. [26] found

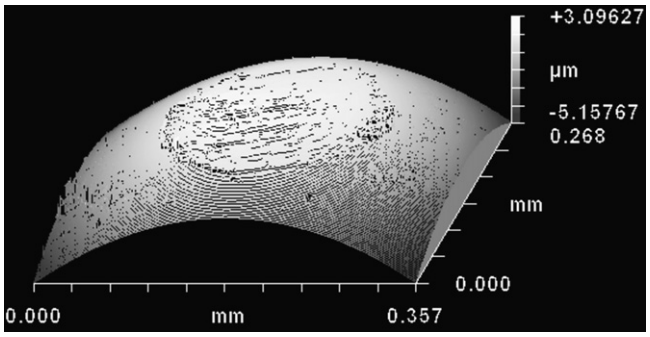

Fig. 8. Non-contact profilometry scan for wear scar on sapphire counterface run against H10.

that rough diamond coatings never achieved low friction but highly polished MCD coatings (Ra < 10 nm) ran-in quickly to $\mu < 0.1$. Similar to the two tests on NCD coating H0 from this study, both previous studies found that MCD coatings resulted in sapphire counterface wear throughout test. Fig. 11 is a plot of the volume of counterface wear versus the roughness of diamond coatings for both the study by Hayward et al. [26] and the data collected here. For MCD samples, the counterface wear had a significant dependence on the initial roughness of the diamond coating. In contrast, for the five NCD coatings studied here, the amount of counterface wear was somewhat independent of coating roughness and was always less than was found for MCD coatings. For the two tests on coating H0 that had higher friction, the counterface wear was greater and more comparable to that found for MCD.

Because Hayward et al. [26] used lower loads (5 N) and different sliding distances from our study, further interpretation of Fig. 11 requires the calculation of wear rates:

$$\mathrm{WR} = \frac{\text{worn volume}}{\text{load} \times \text{sliding distance}} \left(\frac{\mathrm{mm}^3}{\mathrm{N\,m}} \right) \tag{5}$$

For our study, wear rates of the sapphire balls were on the order of 10^{-8} mm^3/(N m). When the ball wore continuously (two tests on H0), the wear rate was 10^{-6} mm^3/(N m). Hayward found higher

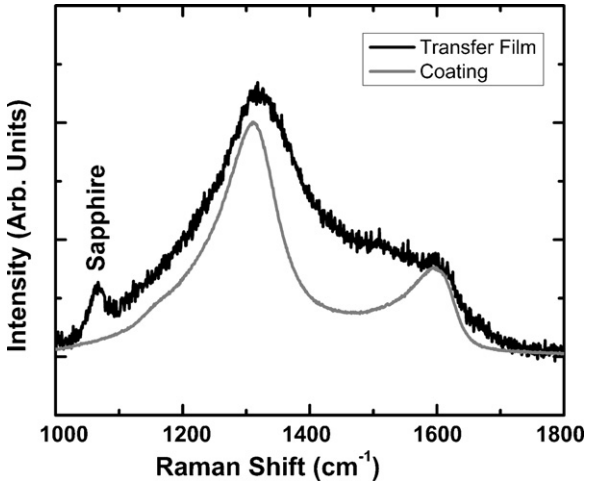

Fig. 9. Raman spectrum from coating H36 and from a transfer film on sapphire from a test run on coating H36.

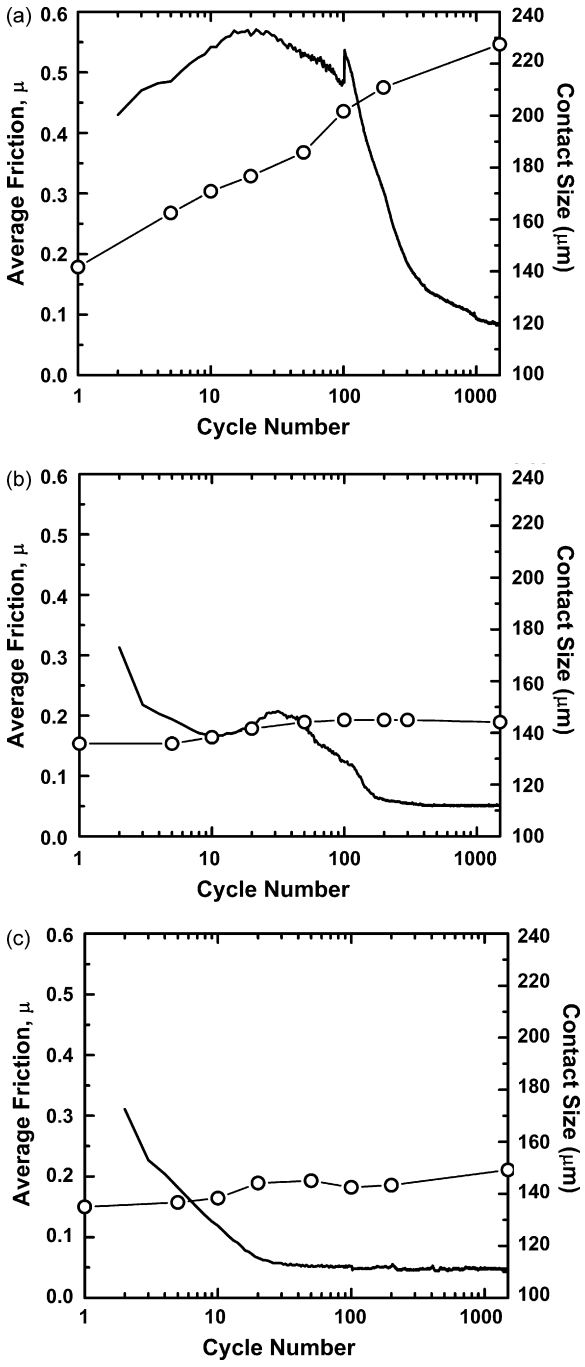

Fig. 10. Friction (solid lines) and contact diameter (open circles) vs. sliding cycle coatings (a) H0, (b) H8.5 and (c) H36.

wear rates, between 10^{-5} and 10^{-2} mm^3/(N m), for sapphire sliding against MCD. Bull et al. [28] also found high sapphire wear rates between 10^{-5} and 10^{-4} mm^3/(N m). Thus, the NCD coatings studied here were found to have significantly different tribological behavior from MCD coatings. In most cases, the sapphire wear took place within the first 50 sliding cycles (see Table 2) followed by interfacial sliding of a carbonaceous transfer film versus wear track with $\mu \sim 0.05$. This is a significant improvement in tribological performance as compared to MCD coatings and is possibly tied to the formation of the transfer film, a phenomenon known to aid in low friction and reduce wear [20,21].

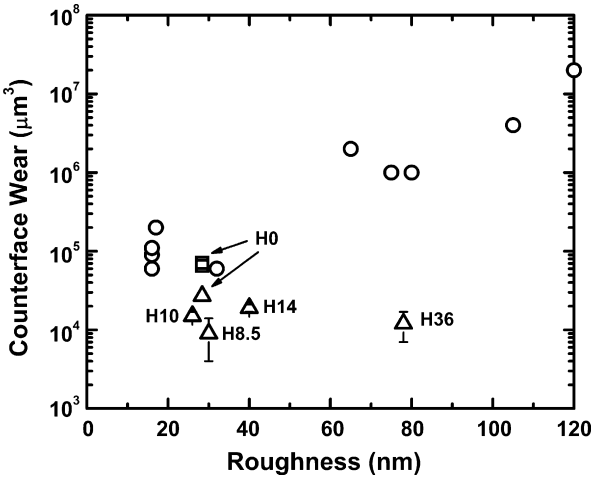

Fig. 11. Counterface wear vs. diamond coating roughness. Open circles are from Ref. [26] with roughness (Ra) calculated from line profiles from contact profilometry. Open triangles are from this work with roughness (RMS) calculated from AFM scans. The square data points are for the two tests on H0 where the counterface wore continuously throughout the test.

The high friction run-in behavior found for our NCD samples is a common feature of NCD coatings [6,10]. Erdemir et al. [10] studied silicon nitride sliding versus NCD and found regimes of high friction followed by $\mu \sim 0.1$ for humid conditions. Similarly, Abreu et al. [6] studied self-mated NCD tribology and found high friction run-in followed by steady-state friction as low as 0.02. For our specimens, the number of cycles to run-in was found to be different for each sample. In some cases, the run-in was very minimal (see H36 in Fig. 5) in comparison to what previous researchers have observed on NCD coatings. Fig. 12 is a plot of the average number of run-in cycles versus NCD coating roughness. Only a weak trend for run-in is found with coating roughness. Coating H36 has the greatest RMS roughness and the shortest run-in. The remainder of the specimens have virtually the same roughness (20–40 nm), but H0 has significantly longer run-in time. Thus, other factors

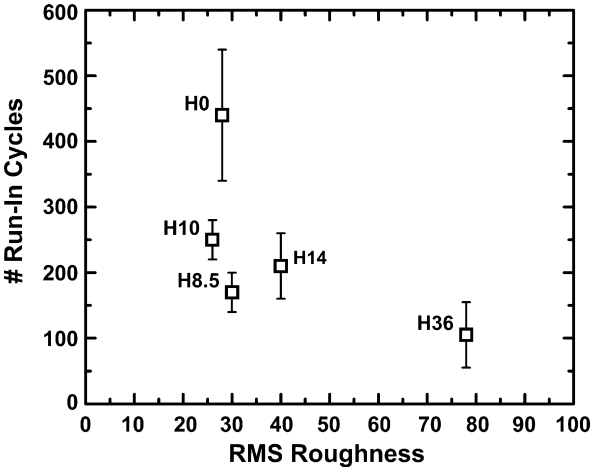

Fig. 12. Average number of run-in cycles vs. NCD coating roughness.

were considered as contributing to the run-in behavior of NCD coatings.

From the X-ray diffraction studies, the grain sizes for both diamond and graphite crystallites were found to be similar for all coatings, but the diamond orientation and graphite content varied from sample to sample (see Table 1). Considering coating texture first, Fig. 13 shows a plot of run-in cycles versus the ratio of the intensity of the diamond (1 1 1) peak to the diamond (2 2 0) peak measured from X-ray diffraction. A trend is observed of decreasing run-in as the preferred crystalline orientation changes from (1 1 0) to (1 1 1). The friction and wear behavior of diamond is known to be anisotropic with the exposed crystal face [24,53,54]. However, our NCD specimens are polycrystalline and the extent of texturing was found to be rather weak. Additionally, based on the work of Enomoto and Tabor [53], the friction anisotropy for diamond typically disappears below a critical contact stress of 20 GPa, a transition point much greater than our contact stress of 0.7 GPa. Therefore, despite the trend found in Fig. 13, crystallographic texture of our diamond coatings is not a likely mechanism for the differences in the observed tribological behavior.

Coating chemistry may also play a role in the run-in behavior. By combining XRD and NEXAFS data we have analyzed the contribution of sp^2 bonded carbon in NCD coatings. NEXAFS data indicated that there was only a small variation in the *total* percent of sp^2 bonded carbon, but a significant change in the energy of the C1s → π* peak position. The total percent reflects both amorphous and crystalline sp^2 carbon while the shift in the peak position has been related to the structure of the sp^2 carbon, with amorphous carbon materials tending to have lower peak position than ordered, graphite-like materials [46,47]. Fig. 14(a) is a plot of the normalized amplitude of the XRD graphite (0 0 2) peak versus the percent sp^2 content as derived from the NEXAFS data. The correlation of these two measurements is weak, with an $R^2 = 0.65$ for a linear fit. This is not surprising since the (0 0 2) XRD peak only corresponds to crystalline graphite, not amorphous. Fig. 14(b) is a plot of relative graphite (0 0 2) XRD peak amplitude versus the C1s → π* peak position from NEXAFS. The coating with no discernable graphite by XRD showed C=C bonding at 285.0 eV, with shifts to 285.5 eV for the films containing increasing amounts of crystalline graphite. We find a linear relationship with $R^2 = 0.93$ between these two values.

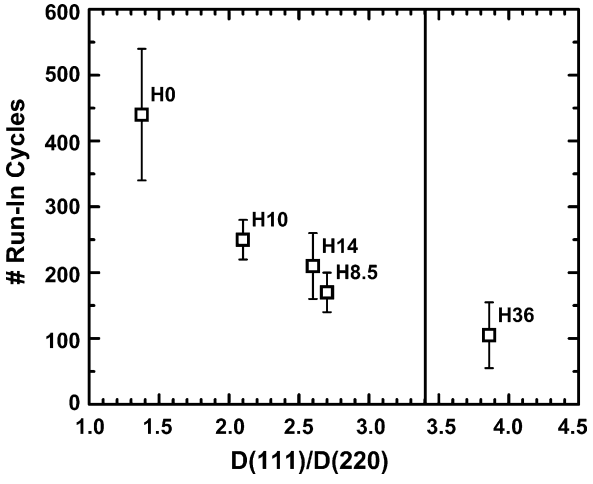

Fig. 13. Average number of run-in cycles versus diamond orientation. The vertical line indicates the D(1 1 1)/D(2 2 0) peak ratio for a coating with no preferred orientation.

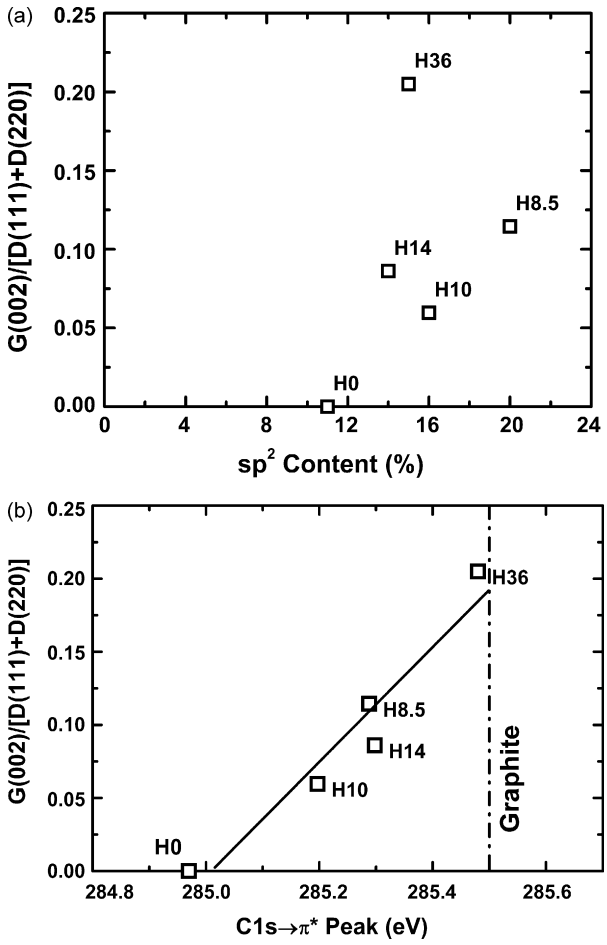

Fig. 14. Plots of the graphite peak (0 0 2) amplitude normalized to the sum of the diamond peak amplitudes [(1 1 1) and (2 2 0)] versus measurements from NEXAFS, including (a) the sp2 content and (b) the position of the C1s → π* peak.

Fig. 15(a) is a plot of the sp^2 content versus run-in cycles. A weak trend toward decreased run-in with increasing sp^2 content is found. Fig. 15(b) is a plot of the normalized (0 0 2) graphite peak from XRD and C1s → π* peak position from NEXAFS

Shifts in C1s → π* peak positions have been attributed to an increase in graphite-like phases for other carbon based films, such as a-CN films under varying growth conditions [55] and flash-annealed ta-C surfaces [56]. However, the detailed nature of the specific bonding configurations that are responsible for the observed peak shift is not known. Gago and co-workers [47] suggest that this downshift in absorption energy of the C1s → π* peak position may be related to either disordered graphitic carbon or sp^2 pairs and/or chains. In our work, we find the energy of the C1s → π* peak position to be correlated to the quantity of graphite crystallites (of a few nm in size) rather than the overall sp^2 content of the coatings estimated from the NEXAFS peak areas.

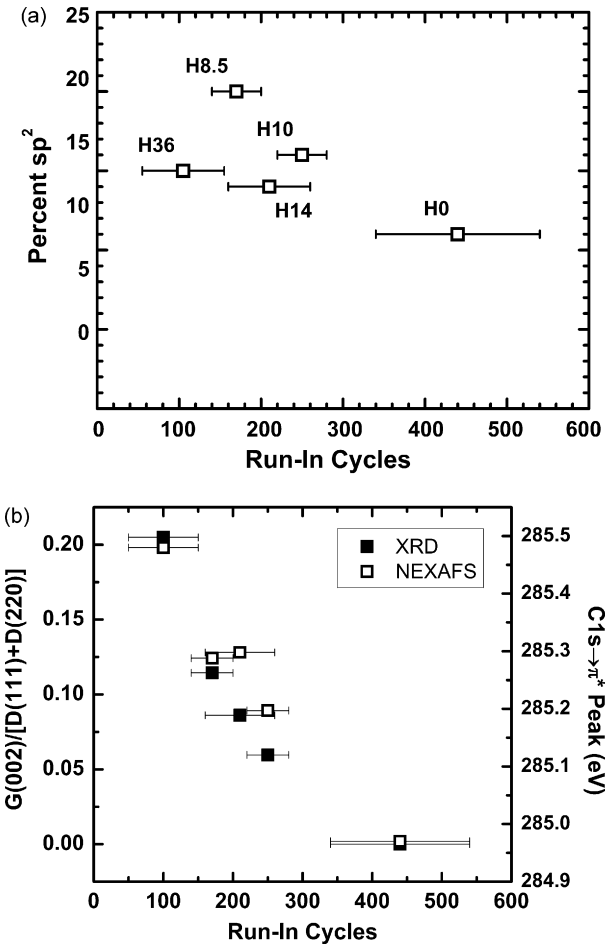

Fig. 15. Plots of coating properties from NEXAFS and XRD versus run-in cycles, including (a) percent sp2 content and (b) normalized graphite peak amplitude and C1s → π* peak position.

versus the number of run-in cycles. These results demonstrate a definite trend between run-in and the graphite content of the film. Sample H0, which had no graphite peak present, had the longest run-in and also had two tests where higher steady-state friction and continuous wear of the sapphire counterface was observed. All other coatings exhibiting this graphite peak had shorter run-in and always exhibited low steady-state friction. Sample H36, with evidence for the highest graphite content, also exhibited a short run-in and in some cases a very quick realization of low friction (see Fig. 5).

The evidence presented here indicates that the degree of crystalline order of the sp^2 bonded carbon in the coating plays a role in the run-in friction behavior of NCD. Based on the current understanding of the structure of NCD [13] prepared by methods similar to those used here, sp^2 bonded carbon exists in the grain boundaries between diamond crystallites, but is typically amorphous. For the coatings discussed here, certain growth conditions led to more order for the sp^2 bonded carbon and also resulted in more rapid run-in to low friction. Exactly how the presence of graphite, an effective solid lubricant material [57], decreases run-in is not known, but may be related to interfacial and transfer film chemistry, or possibly more rapid polishing of the diamond surface. In comparison, the correlation between total sp^2 content in the diamond films and run-in friction was not very strong. Based on the results here, the presence of nanocrystalline graphite, detectable by X-ray diffraction and NEXAFS spectroscopy as a trace amount, appears to have a beneficial effect on the tribological performance of these nanocrystalline diamond coatings.

5. Conclusions

(1) Nanocrystalline diamond coatings exhibited low friction and good wear resistance for sliding against sapphire hemispheres. These beneficial tribological properties were tied to a velocity accommodation mode (VAM) of interfacial sliding between a carbonaceous transfer film and the coating.
(2) *In situ* measurements of the contact diameter correlated well with *ex situ* measurements of counterface wear.
(3) For tests on coatings with evidence of graphite, wear of the sapphire counterface only occurred during the first 50 cycles or less followed by an interfacial sliding process between a carbonaceous transfer film and the wear track.
(4) The tribological performance of nanocrystalline diamond coatings was not influenced by coating roughness over the range studied (20–80 nm).
(5) Friction run-in performance was influenced by coating chemistry and microstructure. A direct correlation between the amount of graphite-structured sp^2 carbon in the NCD films (determined by both XRD and NEXAFS) and decreased run-in cycles to low friction was observed. The shortest run-in times were attained for those films containing the largest graphite-like fraction.
(6) Coating wear was low and found to be polishing in nature. The surface morphology of as-prepared coatings smoothed quickly and the RMS track roughness decreased to below 10 nm during the first 100 sliding cycles.

Acknowledgements

This work has been supported by AFOSR Extreme Friction MURI grant #FA9550-04-1-0381 and the Office of Naval Research. The authors acknowledge Jacqueline Krim at NCSU for program coordination, and Syed Qadri at NRL for assistance with the XRD experiments. The authors are grateful for helpful technical discussions with Nimel Theodore, Robert Carpick and Andrew Konicek. Portions of this research were carried out at the Stanford Synchrotron Radiation Laboratory, a national user facility operated by Stanford University on behalf of the U.S. Department of Energy, Office of Basic Energy Sciences.

References

[1] A.R. Krauss, O. Auciello, D.M. Gruen, A. Jayatissa, A. Sumant, J. Tucek, D.C. Mancini, N. Moldovan, A. Erdemir, D. Ersoy, M.N. Gardos, H.G. Busmann, E.M. Meyer, M.Q. Ding, Ultrananocrystalline diamond thin films for MEMS and moving mechanical assembly devices, Diamond Relat. Mater. 10 (2001) 1952–1961.
[2] A. Richter, R. Ries, R. Smith, M. Henkel, B. Wolf, Nanoindentation of diamond, graphite and fullerene films, Diamond Relat. Mater. 9 (2000) 170–184.

[3] R. Ikeda, M. Hayashi, A. Yonezu, T. Ogawa, M. Takemoto, Fracture observation of polycrystalline diamond film under indentation test, Diamond Relat. Mater. 13 (2004) 2024–2030.
[4] S.J. Bull, Tribology of carbon coatings—DLC, diamond and beyond, Diamond Relat. Mater. 4 (1995) 827–836.
[5] H. Ogi, N. Nakamura, H. Tanei, M. Hirao, R. Ikeda, M. Takemoto, Off-diagonal elastic constant and sp^2-bonded graphitic grain boundary in nanocrystalline-diamond thin films, Appl. Phys. Lett. 86 (2005) 231904.
[6] C.S. Abreu, F.J. Oliveira, M. Belmonte, A.J.S. Fernandes, J.R. Gomes, R.F. Silva, CVD diamond coated silicon nitride self-mated systems: tribological behaviour under high loads, Tribol. Lett. 21 (2006) 141–151.
[7] I.S. Forbes, J.I.B. Wilson, Diamond and hard carbon films for microelectromechanical systems (MEMS)-a nanotribological study, Thin Solid Films 420/421 (2002) 508–514.
[8] Y. Fu, B. Yan, N.L. Loh, C.Q. Sun, P. Hing, Characterization and tribological evaluation of MW-PACVD diamond coatings deposited on pure titanium, Mater. Sci. Eng. A 282 (2000) 38–48.
[9] A.V. Sumant, D.S. Grierson, J.E. Gerbi, J. Birrell, U.D. Lanke, O. Auciello, J.A. Carlisle, R.W. Carpick, Toward the ultimate tribological interface: surface chemistry and nanotribology of ultrananocrystalline diamond, Adv. Mater. 17 (2005) 1039–1045.
[10] A. Erdemir, G.R. Fenske, A.R. Krauss, D.M. Gruen, T. McCauley, R.T. Csencsits, Tribological properties of nanocrystalline diamond films, Surf. Coat. Technol. 120/121 (1999) 565–572.
[11] A. Rajamani, B.W. Sheldon, S. Nijhawan, A. Schwartzman, J. Rankin, B.L. Walden, L. Riester, Chemistry-induced intrinsic stress variations during the chemical vapor deposition of polycrystalline diamond, J. Appl. Phys. 96 (2004) 3531–3539.
[12] J.E. Gerbi, J. Birrell, M. Sardela, J.A. Carlisle, Macrotexture and growth chemistry in ultrananocrystalline diamond thin films, Thin Solid Films 473 (2005) 41–48.
[13] S. Jiao, A. Sumant, M.A. Kirk, D.M. Gruen, A.R. Krauss, O. Auciello, Microstructure of ultrananocrystalline diamond films grown by microwave Ar–CH_4 plasma chemical vapor deposition with or without added H_2, J. Appl. Phys. 90 (2001) 118–122.
[14] Y.K. Liu, P.L. Tso, I.N. Lin, Y. Tzeng, Y.C. Chen, Comparative study of nucleation processes for the growth of nanocrystalline diamond, Diamond Relat. Mater. 15 (2006) 234–238.
[15] Y.C. Lee, S.J. Lin, D. Pradhan, I.N. Lin, Improvement on the growth of ultrananocrystalline diamond by using pre-nucleation technique, Diamond Relat. Mater. 15 (2006) 353–356.
[16] R. Ramamurti, V. Sharlov, R.N. Singh, S. Mamedov, P. Boolchand, Raman spectroscopy study of the influence of processing conditions on the structure of polycrystalline diamond films, J. Vac. Sci. Technol. A 24 (2006) 179–189.
[17] D. Zhou, D.M. Gruen, L.C. Qin, T.G. McCauley, A.R. Krauss, Control of diamond film microstructure by Ar additions to CH_4/H_2 microwave plasmas, J. Appl. Phys. 84 (1998) 1981–1989.
[18] W. Kulisch, C. Popov, On the growth mechanisms of nanocrystalline diamond films, Phys. Status Solidi A: Appl. Mater. Sci. 203 (2006) 203–219.
[19] K. Holmberg, A. Matthews, Coatings Tribology, Elsevier, Amsterdam, 1994, p. 51.
[20] M. Godet, The third-body approach: a mechanical view of wear, Wear 100 (1984) 437–452.
[21] I.L. Singer, S.D. Dvorak, K.J. Wahl, T.W. Scharf, Role of third bodies in friction and wear of protective coatings, J. Vac. Sci. Technol. A (Vac. Surf. Films) 21 (2003) S232–S240.
[22] M.N. Gardos, Tribological fundamentals of polycrystalline diamond films, Surf. Coat. Technol. 113 (1999) 183–200.
[23] S.E. Grillo, J.E. Field, The polishing of diamond, J. Phys. D: Appl. Phys. 30 (1997) 202–209.
[24] S.E. Grillo, J.E. Field, F.M. Van Bouwelen, Diamond polishing: the dependency of friction and wear on load and crystal orientation, J. Phys. D: Appl. Phys. 33 (2000) 985–990.
[25] I.P. Hayward, I.L. Singer, L.E. Seitzman, Effect of roughness on the friction of diamond on CVD diamond coatings, Wear 157 (1991) 215–227.
[26] I.P. Hayward, I.L. Singer, The Tribological Behavior of Diamond Coatings, New Diamond Science, Technology, 1991, pp. 785–789.
[27] I.P. Hayward, Friction wear properties of diamonds and diamond coatings, Surf. Coat. Technol. 49 (1991) 554–559.
[28] S.J. Bull, P.R. Chalker, C. Johnston, V. Moore, The effect of roughness on the friction and wear of diamond thin-films, Surf. Coat. Technol. 68 (1994) 603–610.
[29] B. Bhushan, V.V. Subramaniam, A. Malshe, B.K. Gupta, J. Ruan, Tribological properties of polished diamond films, J. Appl. Phys. 74 (1993) 4174–4180.
[30] H.P. Klug, X-ray Diffraction Procedures for Polycrystalline and Amorphous Materials, Wiley, New York, 1974, pp. 661–665.
[31] G.K. Williamson, W.H. Hall, X-ray line broadening from filed aluminium and wolfram, Acta Metall. 1 (1953) 22–31.
[32] P.K. Bachmann, H.D. Bausen, H. Lade, D. Leers, D.U. Wiechert, N. Herres, R. Kohl, P. Koidl, Raman and X-ray studies of polycrystalline CVD diamond films, Diamond Relat. Mater. 3 (1994) 1308–1314.
[33] L. Fayette, M. Mermoux, B. Marcus, F. Brunet, P. Germi, M. Pernet, L. Abello, G. Lucazeau, J. Garden, Analysis of the fine-structure of the raman line and of X-ray reflection profiles for textured CVD diamond films, Diamond Relat. Mater. 4 (1995) 1243–1250.
[34] L. Fayette, B. Marcus, M. Mermoux, G. Tourillon, K. Laffon, P. Parent, F. Le Normand, Local order in CVD diamond films: comparative Raman, X-ray-diffraction, and X-ray-absorption near-edge studies, Phys. Rev. B 57 (1998) 14123–14132.
[35] F. Silva, F. Benedic, P. Bruno, A. Gicquel, Formation of <1 1 0> texture during nanocrystalline diamond growth: an X-ray diffraction study, Diamond Relat. Mater. 14 (2005) 398–403.
[36] J. Stöhr, NEXAFS Spectroscopy, 1st ed., Springer-Verlag, New York, 1992.
[37] Y. Ufuktepe, G. Akgul, J. Luning, X-ray photoabsorption and total electron yield of Fe thin films at the L_2, L_3 edge, J. Alloys Compd. 401 (2005) 193–196.
[38] T.W. Scharf, I.L. Singer, Role of third bodies in friction behavior of diamond-like nanocomposite coatings studied by in situ tribometry, Tribol. Trans. 45 (2002) 363–371.
[39] E.P. Whitenton, P.J. Blau, A comparison of methods for determining wear volumes and surface parameters of spherically tipped sliders, Wear 124 (1988) 291–309.
[40] A.C. Ferrari, J. Robertson, Origin of the 1150 cm^{-1} Raman mode in nanocrystalline diamond, Phys. Rev. B (Condens. Matter Mater. Phys.) 63 (2001) 121401–121405.
[41] R.J. Nemanich, J.T. Glass, G. Lucovsky, R.E. Shroder, Raman-scattering characterization of carbon bonding in diamond and diamondlike thin-films, J. Vac. Sci. Technol. A 6 (1988) 1783–1787.
[42] S. Prawer, R.J. Nemanich, Raman spectroscopy of diamond and doped diamond, Philos. Trans. R. Soc. Lond. Ser. A (Math. Phys. Eng. Sci.) 362 (2004) 2537–2565.
[43] J. Birrell, J.E. Gerbi, O. Auciello, J.M. Gibson, J. Johnson, J.A. Carlisle, Interpretation of the Raman spectra of ultrananocrystalline diamond, Diamond Relat. Mater. 14 (2005) 86–92.
[44] A.C. Ferrari, J. Robertson, Resonant Raman spectroscopy of disordered, amorphous, and diamondlike carbon, Phys. Rev. B 64 (2001).
[45] A.L. Winfrey, MS Thesis, Nanocrystalline Diamond Deposition for Friction Applications, (North Carolina State University, Raleigh, NC, 2007).
[46] R. Gago, I. Jimenez, J.M. Albella, Detecting with X-ray absorption spectroscopy the modifications of the bonding structure of graphitic carbon by amorphisation, hydrogenation and nitrogenation, Surf. Sci. 482 (2001) 530–536.
[47] I. Jimenez, R. Gago, J.M. Albella, D. Caceres, I. Vergara, Spectroscopy of pi bonding in hard graphitic carbon nitride films: superstructure of basal planes and hardening mechanisms, Phys. Rev. B 62 (2000) 4261–4264.
[48] R.J. Nemanich, S.A. Solin, 1st-order and 2nd-order Raman-scattering from finite-size crystals of graphite, Phys. Rev. B 20 (1979) 392–401.
[49] C. Lenardi, M.A. Baker, V. Briois, L. Nobili, P. Piseri, W. Gissler, Properties of amorphous a-CH(: N) films synthesized by direct ion beam deposition and plasma-assisted chemical vapour deposition, Diamond Relat. Mater. 8 (1999) 595–600.

[50] G. Cicala, P. Bruno, F. Benedic, F. Silva, K. Hassouni, G.S. Senesi, Nucleation, growth and characterization of nanocrystalline diamond films, Diamond Relat. Mater. 14 (2005) 421–425.
[51] I.L. Singer, Solid lubrication processes, in: I.L. Singer, H.M. Pollock (Eds.), Fundamentals of Friction, Macroscopic and Microscopic Processes, Netherlands, 1992, pp. 237–261.
[52] K.J. Wahl, I.L. Singer, Quantification of a lubricant transfer process that enhances the sliding life of a MoS_2 contact, Tribol. Lett. 1 (1995) 59.
[53] Y. Enomoto, D. Tabor, The frictional anisotropy of diamond, Proc. R. Soc. Lond. Ser. A: Math. Phys. Eng. Sci. 373 (1981) 405–417.
[54] J.R. Hird, J.E. Field, Diamond polishing, Proc. R. Soc. Lond. Ser. A (Math. Phys. Eng. Sci.) 460 (2004) 3547–3568.
[55] R. McCann, S.S. Roy, P. Papakonstantinou, M.F. Bain, H.S. Gamble, J.A. McLaughlin, Chemical bonding modifications of tetrahedral amorphous carbon and nitrogenated tetrahedral amorphous carbon films induced by rapid thermal annealing, Thin Solid Films 482 (2005) 34–40.
[56] D. S. Grierson, A. Konicek, R. W. Carpick, Personal Communication, October 10, 2007.
[57] F.P. Bowden, D. Tabor, The friction and Lubrication of Solids, Clarendon, Oxford, 1986.